Applied Surface Science 40 (1990) 349–358
North-Holland

THE Ti/c-Si SOLID STATE REACTION
II. Additional measurements by means of RBS, XPS and AES

J.M.M. DE NIJS * and A. VAN SILFHOUT

Department of Solid State Physics, University of Twente, P.O. Box 217, 7500 AE Enschede, The Netherlands

Received 28 February 1989; accepted for publication 9 October 1989

In a previous paper [Appl. Surface Sci. 40 (1990) 333], we have reported the results of a spectroscopic ellipsometric study of the c-Si/Ti solid state reaction. For this purpose we have grown and heated thin (~ 10 nm) Ti films on a clean c-Si substrate. The investigation revealed that already at moderate temperatures a metastable silicide (~ 350 °C), probably a monosilicide, and disilicide (~ 450 °C) are formed. These two metastable transition states, denoted by state I and II respectively, and the final disilicide (state III, ~ 700 °C) are additionally studied by means of a number of quantitative techniques, such as RBS, XPS and AES. The results reveal a Si-enriched monosilicide state I, Si : Ti = 1.2 and a stoichiometric, but Si segregated disilicide state II; surface composition approximately $TiSi_3$. The finally obtained disilicide (III) has recrystallized into probably large, flat islands embedded in a c-Si matrix.

1. Introduction

In a short series of three articles, we report on the result of an extended study of the c-Si/Ti solid state reaction. This is the second paper dealing with the quantitative analyses of the previously identified metastable intermediate states and the final state.

In the preceding paper, we have described the optical experiments and the results. Thin (~ 10 nm) Ti films have been grown on top of a clean c-Si(111) substrate inside an UHV system. These layers are slowly heated, meanwhile following the intermixing process by means of three-wavelength ellipsometry, $\lambda = 340$, 450 and 550 nm. These ellipsometrical registrations revealed the occurrence of some reordering processes in the as-deposited Ti layer, two metastable intermediate states (I and II) and a final transition at ~ 700 °C (III). Spectroscopic ellipsometry ($E = 2.0$–4.5 eV) has been applied to characterize these intermediate states and the as-deposited Ti layer. Analysis of the ellipsometrical spectra of the as-deposited layers unambiguously show that a thin (~ 3 nm) intermixed Ti–Si layer is formed prior to the growth of a pure Ti layer. When the layer is slightly heated, ~ 175 °C, we observed a continued intermixing at the metal/silicon interface and a reordering of the Ti atoms in the as-deposited metal layer. Increasing the temperature enhances the Si indiffusion, as at ~ 350 °C it was possible to obtain a completely converted intermediate state. This metastable phase is denoted by state I. Analysis of the optical data revealed a strongly inhomogeneous layer with a composition of approximately TiSi. At ~ 400 °C, a second Si indiffusion into the silicide layer is initiated, ultimately yielding at ~ 450 °C a homogeneous disilicide, state II. From additional studies reported in the literature [2–5], it is concluded that the disilicide obtained should have the metastable C49 structure. A final transition (state III) is observed at ~ 700 °C. Analysis of the ellipsometrical spectrum indicates a large amount (~ 20%) of c-Si precipitates in the silicide top-layer.

In this paper we will present the results of a number of additional measurements. The UHV system in which we have grown and heated the

* Present address: Department of Physics, Eindhoven University of Technology, P.O. Box 513, 5600 MB Eindhoven, The Netherlands.

layers, is equipped with Auger electron spectroscopy (AES) with a retarding field analyzer. This system offered us the possibility to study the surface composition of a number of specially prepared samples in-situ. With great care we have prepared two samples that are optically identical to the metastable phases I and II. The samples and the sample which is used for the previous presented [1] optical analyses (sample III) are subjected to an X-ray photoelectron-emission spectroscopy (XPS) study and Rutherford backscattering (RBS) measurements. The RBS results fully support the results previously obtained by spectroscopy ellipsometry [1]; the low-temperature ($\sim 350\,^{\circ}$C) monosilicide phase (sample I) has a composition of $TiSi_{1.2}$, the moderate temperature disilicide (sample II) is almost stoichiometric ($TiSi_{2.1}$) whereas a strongly Si-enriched disilicide is found for the sample III, $TiSi_{2.4}$.

The results obtained by means of the surface-sensitive techniques, XPS and AES AES, reveal a large discrepancy between the bulk and surface composition. Both disilicides are more or less silicon segregated; the disilicide sample II has a surface composition of $TiSi_{2.8}$, the final state is almost covered by a pure Si layer, composition $TiSi_7$.

Sample II has also been subjected to an AES Ar^+ depth profiling study. This study confirms the results of the in-situ AES, XPS and RBS investigations.

This paper is organized as follows. Firstly we will treat the in-situ AES measurements. The preparation of the reference samples I, II and III will be described in section 3. Subsequently in sections, 4, 5 and 6 we present respectively the XPS study, the RBS investigation and the AES Ar^+ depth profiling. The paper closes with a discussion on the presently and previously obtained results.

2. In-situ Auger analyses

A number of metastable monosilicide (I, $\sim 350\,^{\circ}$C) and low-temperature (C49) disilicide samples (II, $\sim 450\,^{\circ}$C) have been investigated by means of in-situ AES. Prior to these measurements, we have calibrated the Si LVV and Ti LMM peak-to-peak heights on the clean Si sample and an evaporated Ti layer respectively [6,7]. A beam of 2 keV electrons and 1.25 μA total current has been used. The spectra are recorded by a retarding field analyzer in the dN/dE mode.

Table 1
Normalized Si LVV and Ti LMM peak-to-peak height ratios for the metastable monosilicide and the low-temperature (C49) disilicide

Samples	Peak-to-peak height ratios		Estimated atomic ratio $N_{Si} : N_{Ti}$
	Ti	Si	
Monosilicide	0.45 ± 0.05	0.50 ± 0.1	1.1 ± 0.3
Disilicide (C49)	0.25 ± 0.05	0.70 ± 0.1	2.8 ± 0.5

In table 1 we have enlisted the results of the AES measurements of the samples I and II. For both, Ti and Si, it presents the peak-to-peak height ratios of the measured and the reference peaks, and the experimental scatter as estimated from the variance among the different samples.

The peak-to-peak height ratios clearly reveal an increase of the Si concentration observed at the surface, whereas the Ti amount is reduced. Striking is the large variance of the peak-to-peak height ratios, indicating that an unambiguous, stoichiometric surface composition is not obtained. However, intermediate state I appears to have a composition more or less TiSi-like, whereas intermediate state II corresponds to a Si-enriched $TiSi_2$ phase. These results are in good agreement with those reported by Idzerda et al. [8]. Further, such a Si segregation is observed also in the case of an annealed, cosputtered $TiSi_2$ layer above a Si substrate [9].

3. Samples I, II and III

The ex-situ study of the intermediate states I and II of the silicide formation that we have distinguished in the first paper of this series, requires a number of carefully prepared samples which are equivalent to these intermediate states. The sample discussed in the previous article [1] provides us the final-state sample, sample III. The samples identical to the metastable phases I and II

Table 2
Comparison of samples I and II with the metastable monosilicide and the C49 disilicide, respectively

Sample	Top-layer		Second-layer		Residue
	Thickness (nm)	fraction (%)	Thickness (nm)	fraction (%)	
I	3.0±3	0.98±0.1	15.7±3	0.95±0.01	0.005
II	1.8±3	0.90±0.1	25.2±3	1.00±0.01	0.003

A two-layer model where both layers are allowed to contain a variable amount of voids is used. Sample I is fitted by means of LRA with the dielectric function ϵ_I and sample II with ϵ_{II}. The table lists of the optimized thicknesses, the metal fractions and their confidence limits. The residues obtained warrant that the samples I and II are equivalent to the intermediate states 1 and 2.

had to be prepared. For this purpose we grew ~ 10 nm thick Ti layers on clean, reconstructed Si(111) substrates. These layers were subsequently annealed up to the temperatures of 350 and 450 °C for the samples I and II, respectively. The process was followed by the ellipsometer and the heating was stopped once the different, distinguishable processes had ceased. Prior to and after the heating spectroscopy ellipsometric scans were made for a proper optical comparison between these samples and the previously distinguished intermediate states.

Table 2 shows the optical analyses of samples I and II. Sample III is the same sample as the one presented in the previous paper [1] and from which we have derived the reference dielectric functions for the metastable monosilicide and the low-temperature C49 disilicide, $\tilde{\epsilon}_I$ and $\tilde{\epsilon}_{II}$, respectively. A two-layer model where both layers are allowed to contain a variable amount of voids, is used. Sample I shows to be homogeneous and a one-layer model should suffice. Sample II exhibits a slightly lower silicide concentration at the surface, which suggests some surface roughness.Confidence limits for the thicknesses are quite large (±3 nm for d_1 and d_2) because of the strong correlation between the two layers. Confidence limits for the void fractions are for both samples 0.10 and 0.01 for respectively the top and second layer. The residues of both fits are extremely low, warranting that the dielectric functions used are the appropriate ones, and we can safely conclude that the samples I and II are identical to the intermediate states I and II as observed during the annealing of sample III.

4. X-ray photoelectron spectroscopy

We have studied the samples I, II and III by XPS. The objective was to obtain an unambigious characterization of the samples. Both, chemical state of the Ti/Si samples and their quantitative surface composition were questioned [6,7,10,11]. The results, however, will show to be quit poor. Shifts of E_B are hardly observed, probably because of the particular character of the chemical bonding and electronic structure of the Ti/Si system. The composition could be obtained, but it required quite an effort to eliminate the peak-area distortion due to a negative oxide layer grown upon exposure to the air.

Subsequent to the preparation, the samples were transferred to the XPS system, which, unfortunately, requires the exposure of the samples to the air. The analyses were performed on the Kratos XSAM-800 system, equipped with a Mg Kα (E = 1253.6 eV) Röntgen source and a concentric hemispherical analyser at constant pass energy (20 eV).The background of inelastically scattered electrons was subtracted from the spectra by the method of Shirley [12]. This method is questionable [13], it may introduce errors in the absolute peak positions and the peak areas, but presently there is no better alternative available. Prior to any measurement the energy scale was calibrated with the Cu 2p peak (E_B = 932.67 eV) and the Cu LMM Auger peak (334.95 eV).

The most pronounced photoelectron excitations for titanium and silicon involve 2p core levels. Concerning metal Ti, the $2p_{1/2}$ and the $2p_{3/2}$ core levels are separated enough to observe them as two distinct peaks in the XPS spectrum near $E_B \approx$ 459.7 and $\approx$ 454.0 eV, respectively. The Si 2p levels cannot be distinguished and a single peak is found at $E_B \approx$ 99.1 eV. XPS spectra were recorded for the samples I, II and III and for pure Si and Ti samples covered by their native oxides.

In the finally obtained XPS spectra, contributions are found that belong to the oxide layer and the bulk silicide. Our aim is to obtain the bulk

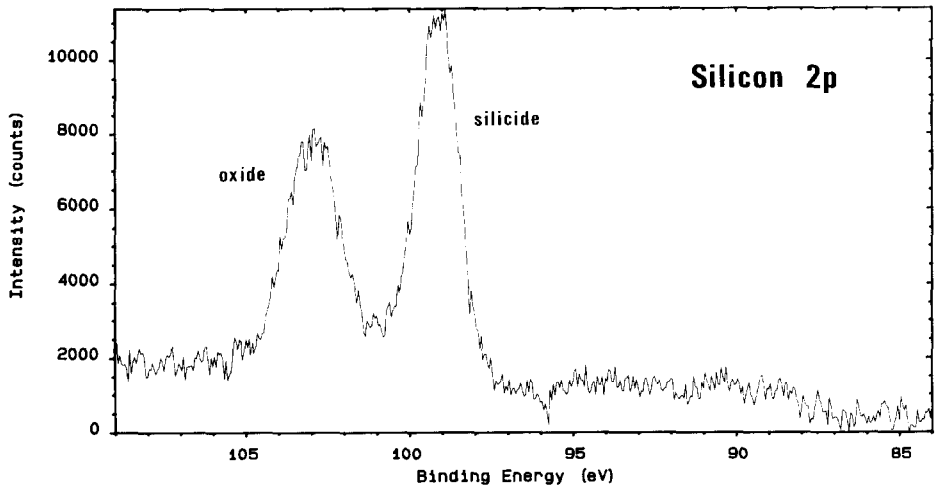

Fig. 1. XPS spectrum of Si in sample II.

Ti–Si peak-area ratio which requires a proper separation of the oxide and silicide contributions to the XPS spectra. The peak-area ratio obtained after the separation of the bulk and oxide contributions still has to be corrected for the distortion due to the oxide layer. For this purpose, measurements are performed for two photoelectron escape angles, 0° and 40°, as measured from the surface normal. These two measurements shall allow us to calculate the correct peak-area ratio in the absence of the oxide layer.

The spectra for Si and Ti as recorded on sample II are displayed in figs. 1 and 2. The silicon spectrum shows two dominant peaks, one at $E_B \approx$ 99.1 eV, which is attributed to the silicon beneath the oxide layer, and one at $E_B \approx 103.0$ eV due to the oxide. The sub-oxides are found in between of these two peaks. The spectrum as displayed in fig. 2 shows the Ti $2p_{1/2}$ and $2p_{3/2}$ silicide peaks as well as the Ti oxide peaks. One should expect to find four peaks, however, the Ti $2p_{3/2}$ oxide peak and the Ti $2p_{1/2}$ silicide peaks fall on top of each

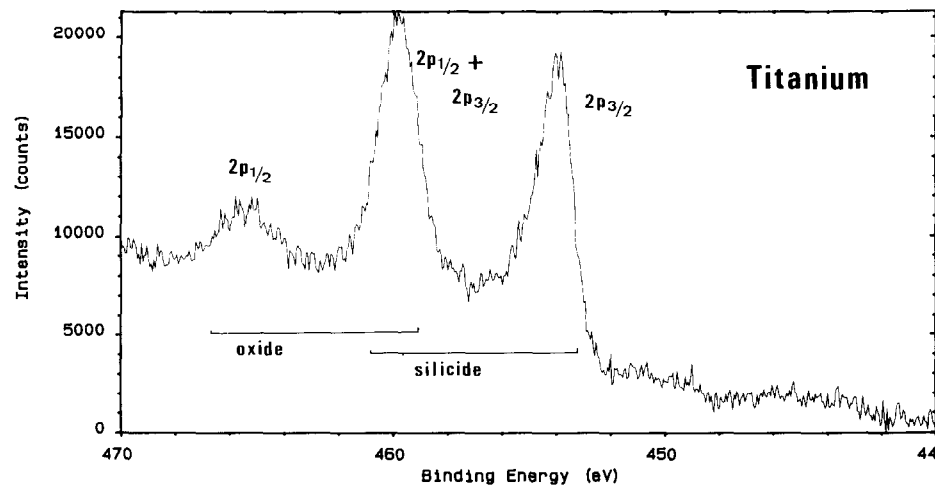

Fig. 2. XPS spectrum of Ti in sample II.

other and the total spectrum apparently exhibits but three peaks.

The qualitative analysis of the peaks comprises the actual binding energies.These energies are expected to reflect the chemical environment of the constituting atoms, for example, one can easily distinguish the Ti in a pure metal layer from that in an oxide. Although this technique generally yields satisfying results, we have to report that we did not observe any significant shift of E_B for Si or Ti in the various samples. Certainly, the measurements are obstructed by the oxide layer, nevertheless, it can be concluded that the core levels involved do not experience a large change of their electronic environment due to the silicide formation.

The binding-energy shifts are dominant by two mechanisms, (1) the ability of electronic relaxation of the valence electrons upon the creation of a core-hole and (2) the actual electrical potential of the core-electron due to the charge density of the valence electrons. The first and the latter are commonly referred to as the final-state and initial-state effect and are extensively discussed in the review articles of Egelhoff [14] and Shirley [15]. The large shift of the photoelectron binding energy of, for example, Ti upon the formation of TiO_2, thus can be attributed to the redistribution of the valence electrons – the Ti valence electrons are attracted to the oxygen atoms – and a reduction of the screening of the core-hole due to the conversion from a conductor (metal) to an insulator (oxide). It will be obvious that since the silicide formation does not involve a large charge redistribution as compared to the formation of an oxide whereas the electrical properties are less affected too, the binding-energy shift will be small. In particular, when considering the shifts upon the conversion from a monosilicide to a disilicide, one can expect but a very small shift of E_B. However, the fact that this shift is presently not observed does not necessarily preclude silicide formation.

Although the results of the binding energy shifts are quite meager, we can still perform the quantitative analyses of the surface composition. The objective is to determine the composition of the silicide, however, this is obstructed by the presence of a thick (~ 3 nm) oxide layer. In general, one can calculate the atomic ratio of the constituent components from the peak areas. The problem is that the silicide peak areas are reduced by inelastic electron scattering in the oxide overlayer. The loss rate of inelastically scattered electrons is energy dependent and, consequently, the peak-area ratio is not conserved during the photoelectron transport through the oxide layer. The loss rate of the photoelectrons is expressed in terms of the escape depth.

The relative attenuation of the peak-area ratio (ϑ) is expressed by

$$\vartheta(d, \phi) = \vartheta^0 \exp\left[-\frac{d}{\cos\phi}\left(\lambda_{Ti}^{-1} - \lambda_{Si}^{-1}\right)\right],$$

$$\vartheta(d) = I_{Si}(d)/I_{Ti}(d), \qquad (1)$$

where λ, d and ϕ denote respectively the escape depth of the photoelectrons, the thickness of the oxide layer and the photoelectron escape angle. ϑ^0 is the ratio when the surface layer is absent, which is the objective. The escape depth, λ, is governed by the kinetic energy (E_K) of the electron and can be described by a simple formula [6,7,16]. Nevertheless, this formula is very tentative since it is strongly material dependent [17–20]. Commonly, in the absence of surface layers, this material dependency can be omitted [10,21], but in the present case of a thick oxide layer this can lead to erroneous results. Hence, we cannot directly apply eq. (1) because we do not have reliable values for the escape depth at our disposal nor do we know the thickness of the oxide layer. These problems can be surmounted and the influence of the oxide layer can be eliminated from the peak-area ratio by means of a second measurement at another escape angle. The exponential factor of eq. (1) can then be obtained from the quotient of the peak-area ratios at $\phi = 0°$ and $\phi = 40°$. Expressed in the measured quantities we find for the undistorted peak-area ratio ϑ^0:

$$\vartheta^0 = \vartheta(d, 0)\frac{\vartheta(d, 0)^\chi}{\vartheta(d, \phi)}, \quad \chi = \frac{\cos\phi}{1 - \cos\phi}. \qquad (2)$$

Application of this formula requires a correct separation of the oxide and the silicide contributions in the spectra. This can be accomplished by means of peak synthesis of the spectra. The main

Table 3
Corrected Si–Ti peak-area ratios, $I_{Si} : I_{Ti}$, for the different samples; application of appropriate relative sensitive factors yields the atomic ratio

Sample	Corrected peak-area ratio	Atomic ratio $N_{Si} : N_{Ti}$
I	0.28	1.2
II	0.62	2.7
III	1.60	7

problem concerns the suboxides observed between the oxide and the silicide peaks. However, their relative positions as measured from the oxide binding energy are known from the literature [22–27] and we have adopted these results to fix the position of the Gaussians that correspond to the Ti and Si suboxides.

Some special attention has to be paid to the synthesis of the Ti $2p_{1/2}$ and $2p_{3/2}$ peaks. These $2p_{1/2}$ and $2p_{3/2}$ levels are isolated from the valence levels and thus experience their electrical environment and detection quite similarly. Thus, the binding energy difference of the $2p_{1/2}$ and $2p_{3/2}$ photoelectrons does not depend on the chemical or electronic state of the atom and the area ratio of the 2p peaks is determined solely by the cross-section ratio for XPS photo-ionization of the $2p_{1/2}$ and $2p_{3/2}$ levels. It is for this reason that the Ti $2p_{1/2}$ and $2p_{3/2}$ peaks that correspond with one chemical state are fitted with a fixed peak-area ratio and a fixed photoelectron binding-energy difference of 5.7 eV. The peak-area ratio and the binding-energy difference are obtained from a pure titanium sample. The peak-area ratio $I_{3/2} : I_{1/2} = 2.2 : 1$ is found, which clearly reflects the electron occupation of the levels [28,29]. The slight disagreement is probably an indication for the ambiguity of the background subtraction.

Peak synthesis and the separation of the oxide, suboxide and silicide contributions are performed as discussed above. Peak-area ratios for the Ti and Si silicide contributions are calculated for both escape angles. In table 3 we have summarized the final, corrected peak-area ratios of the various samples as calculated by means of eq. (2). The atomic ratios $N_{Si} : N_{Ti}$ are subsequently calculated from the undistorted peak-area ratio and the appropriate relative sensitivity factors of Ti and Si [7,10].

Regarding samples I and II, we note that the atomic ratios at the surface agree excellently with the in-situ Auger measurements, see table 1. Remarkable is the very high Si concentration observed at the surface of sample III – probably the surface is covered by a Si overlayer. Such an overwhelming surface segregation is observed previously by Kuiper et al. [9].

5. Rutherford backscattering

Samples I, II and III were investigated by means of Rutherford backscattering (RBS) [30]. This method offers the best possibility for the unambiguous determination of the bulk composition and it yields an estimation of the thickness at the same time. The experiments are performed with a 2 MeV He ion beam at normal incidence and at a scattering angle of 170°.

Fig. 3 displays the RBS spectra as they were recorded for the three samples. The spectra were analyzed by the simulation program RUMP [31], which yields an interpretation of the spectra in terms of a stack of smooth, homogeneous layers

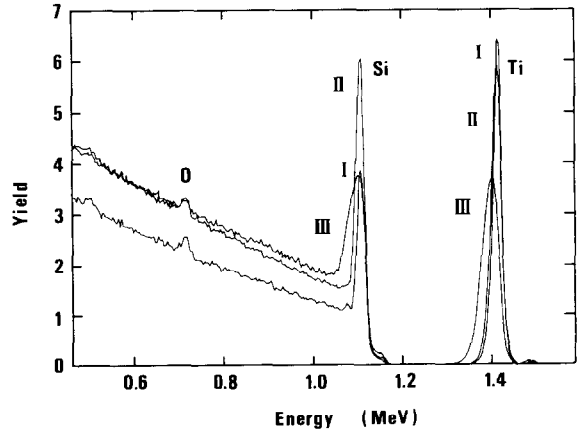

Fig. 3. RBS spectra for the samples I, II and III.

Table 4
Composition and thickness of the silicide layers of the samples I, II and III

Sample	Silicide layer	
	d (nm)	Atomic ratio $N_{Si} : N_{Ti}$
I	20	1.2
II	25	2.1
III	50	2.35

These results are obtained from the analysis of the RBS spectra by means of RUMP. The oxygen in the oxide overlayer is not listed. Sample III required two layers for a correct simulation, apart from a homogeneous silicide layer, a 7 nm thick pure SiO_2 layer was needed.

on top of a substrate. Regarding the samples I and II, a single layer containing Si, Ti and O sufficed to simulate the spectra. In the case of sample III, two layers were required, a pure SiO_2 layer above a Si–Ti mixed layer. The results are summarized in table 4.

Sample I is a Si-enriched monosilicide, the thickness is supported by the optical analyses, see table 1. Sample II is a slightly enriched disilicide, hence it shows unambiguously that a disilicide can be grown at temperatures as low as ~ 450 °C. The thickness is slightly less than 27 nm, which was found from the LRA. The results show further that sample III has likely a pure SiO_2 top-layer and, therefore, the initial surface had to be Si segregated. This result agrees well with the XPS observation from the previous section. Below this segregation region, there occurs a strongly Si-enriched $TiSi_2$ layer. The shape of the RBS peaks of sample III has become asymmetric, showing that the layer is not as flat as those observed for the other samples I and II. The thickness, ~ 50 nm, gives the posterior confirmation that the layer is too thick to allow its determination by means of optical methods; the information depth as been exceeded [1]. The amount of Si in the layer as it emerged from the optical analysis is slightly larger than the present result. This, however, can be attributed to the Si enrichment at the surface.

These and the previous results suggest that the heating at 700 °C has probably yielded a top-layer of large, flat $TiSi_2$ crystals embedded in a c-Si matrix. The Si layer above the crystallites has to be very thin or it lacks the optical characteristics of covalently bonded Si, for example because it has the metallic $sp^2 2s^2$ configuration, since there is no positive indication for such a layer from the linear regression analysis [1].

6. AES Ar^+ depth profiling

Sample II has been investigated by Auger depth profiling [6,7]. The objective was to study the homogeneity of the mixed layer and to obtain the atomic composition as it is measured by AES.

The measurement was performed on a Perkin-Elmer PHI 600 system. A beam of 10 keV electrons and a total current of 0.5 μA had been applied. During the Ar^+ sputtering ($E_K = 3.5$ eV), the Ti LMM, Si LVV, Si KLL, O KLL and the C KLL Auger peak-to-peak (p–p) heights were recorded. In fig. 4 we present the thus obtained (p–p) values of the elemental peaks investigated.

An independent calibration of the sputter rate on a Ta_2O_5/Ta sample with the same sputter conditions, yielded a sputter rate of 4.3 nm/min. Although the sputter yields of Ti, Si and Ta are comparable [7], it cannot be advised to consider this sputter rate but as a rough estimation. Employing the information on the layer thickness, table 2, we find a sputter rate of about 3.5 nm/min. Preferential sputtering needs not to be considered, as shown by Kuiper et al. [9].

Displayed in fig. 5 is the atomic concentration profile as calculated from the Ti and Si (p–p) values. The relative sensitivity factors are taken

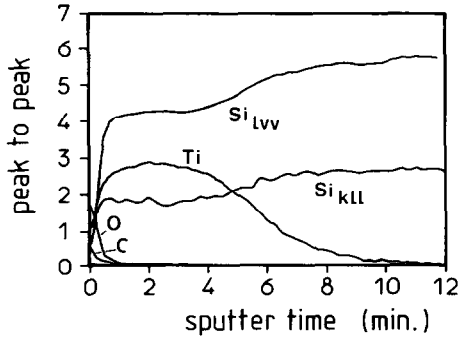

Fig. 4. Auger Ar^+ sputter profile of sample II. The figure displays the peak-to-peak values.

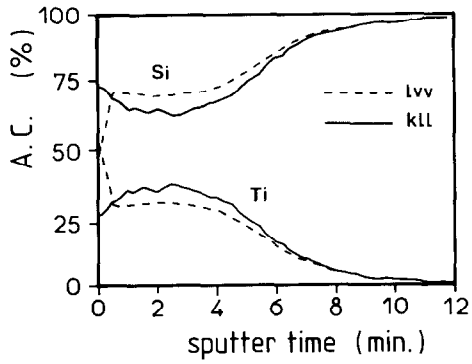

Fig. 5. Auger Ar^+ sputter profile of sample II. The figure shows the concentration profiles.

from the Perkin-Elmer handbook [32]. Upon studying fig. 5, one firstly notes the striking disagreement between the composition profiles as obtained from the Si LVV and the Si KLL (p–p) values; the first reveals a Ti segregation whereas, according to the second, there should be a Si enrichment at the surface. In the case of the Si LVV based profile, the Si (p–p) value is strongly affected by the peak shape; initially an oxide as well as a silicide contribution is present in the dN/dE spectrum, which broadens and flattens the Si LVV peak. Both contributions are not distinguished properly by the operating program, which, as a consequence, yields a (p–p) ratio below its actual value. Hence, we have reason to believe that the atomic Si/Ti ratio in the presence of the oxide layer is too low in the case of the Si LVV derived profile and that, initially, the Si KLL based profile resembles mostly the actual composition. One should note that the initial composition as derived from the Si KLL peak, agrees well with the in-situ measured results for the state-II-like samples and the XPS study. See tables 1 and 3. Further, the observed surface segregation of Si extending ~ 3 nm is in excellent agreement with a similar study of Kuiper et al. [9].

The sputter profile does not reveal a sharp silicide/silicon interface, which is quite common due to the finite escape depths involved and the mixing and surface roughening caused by the Ar^+ sputtering. Presently, we observe a transition region (80%–20% Ti concentration) of about 11 nm. In the preceding calibration of the sputter rate on Ta_2O_5/Ta, the sharp interface blurred over ~ 8.5 nm. Apparently, we can attribute the transition region mainly to the sputter process, however, there is no evidence for an atomically sharp interface and a thin mixed region (2–4 nm) could be expected.

From the arguments presented above, we conclude that the silicide layer is homogeneous but that is Si enriched at the surface whereas an transition layer at the silicide–silicon interface cannot be excluded.

If we, finally, consider the atomic composition, there appears to be a quantitative difference between the composition calculated from the Si LVV–Ti (p–p) ratio and the Si KLL–Ti (p–p) ratio, the first yielding an atomic Si to Ti ratio $N_{Si} : N_{Ti} = 2.3$, and the latter $N_{Si} : N_{Ti} = 1.8$. Both values indicate a titanium disilicide, but it can not be concluded with certainly whether it is Si or Ti enriched.

7. Discussion and conclusion

The additional measurements have confirmed what was already expected from the optical analyses of the preceding article. The complete picture that emerges from these results can now be summarized as follows.

The first Ti atoms that condensed on the Si substrate react with the silicon and a monosilicide layer is formed. This intermixing sustains as long as there is enough free silicon available. Upon the formation of ~ 3 nm monosilicide, the lack of silicon terminates further growth of an reacted silicide layer and a pure Ti layers continues growing.

Commencing the heating at ~ 200 °C permits the Ti atoms in the top-layer to reorder to some extent. Meanwhile, Si diffusion is initiated and the intermediate layer proceeds to grow. At $T \approx$ 350 °C all Ti is consumed and a monosilicide phase is formed. Quantitative analysis has shown that this monosilicide is Si enriched and far from homogeneous. This inhomogeneity has to be at-

tributed to a strong gradient of the Si concentration, which, since the phase field of the monosilicide is quite flat [2], is required to bring about a substantial Si transport during the growth of the mixed layer. The observation of such a large Si gradient in a similar sample, is recently confirmed by Raaijmakers [2]. Structure analyses by Raaijmakers have also shown that this monosilicide lacks any atomic ordering; it is an amorphous compound.

Continuing the heating initiates a second Si in-diffusion and a $TiSi_2$ phase nucleates.The optical analysis has shown that this layer is homogeneous as compared to the preceding monosilicide. Nevertheless, the Auger and XPS measurements reveal a slightly Si segregated surface, its composition being close to $TiSi_3$. This disilicide is known to have a crystalline C49 structure [2–5].

Finally, at $\sim 700\,^{\circ}C$ we observe a last transition. A roughened layer is formed which has a large surplus of crystalline Si. Probably, the top-layer consists of large, flat $TiSi_2$ C54 grains embedded in a c-Si matrix. Stress is observed in this c-Si. Although a strong surface segregation of Si is found, it is not likely that it exhibits c-Si characteristics since the presence of c-Si top-layer did not show from the LRA. Either the layer is too thin, or the Si has metal-like (2s2p) configuration.

In the context of these results, we will shortly discuss the work of Raaijmakers [2]. He has studied the $TiSi_2$ formation from cosputtered Ti–Si layers, from stacked systems comprising Ti and a-Si layers and from Ti layers sandwiched between c-Si and a-Si. Raaijmakers has found similar kinetics for the Ti/c-Si and Ti/a-Si solid state reaction. In both cases an amorphous monosilicide grows at $\sim 400\,^{\circ}C$. This layer exhibits a large Si concentration gradient as observed presently [1]. Continuing the heating entails a second Si in-diffusion and C49 $TiSi_2$ nucleates at $\sim 500\,^{\circ}C$ for Ti/a-Si and somewhat higher (525–550 °C) for Ti/c-Si. Finally, at $\sim 800\,^{\circ}C$ the transition of the C54 structure is observed. In the present study we have found temperatures that are slightly less than those of Raaijmakers, however the kinetics observed fully support the presently obtained sequence of phases.

Acknowledgements

We kindly thank Dr. A.E.T. Kuiper from Philips Research Laboratories for his support of the RBS measurement.

References

[1] J.M.M. de Nijs and A. van Silfhout, Appl. Surface Sci. 40 (1989) 333.
[2] I.J.M.M. Raaijmakers, Fundamental Aspects of Reactions in Titanium Silicon Thin Films for Integrated Circuits, PhD Thesis, Eindhoven (1988).
[3] R. Beyers and R. Sinclair, J. Appl. Phys. 57 (1985) 5240.
[4] I.J.M.M. Raaijmakers, A.H. Reader and H.J.W. van Houten, J. Appl. Phys. 61 (1987) 2527.
[5] W. Bretschneider, G. Beddies and R. Scholz, Thin Solid Films 158 (1988) 255.
[6] L.C. Feldman and J.W. Mayer, Fundamentals of Surface and Thin Film Analysis (North-Holland, New York, 1986).
[7] D. Briggs and M.P. Seah, Practical Surface Analysis by Auger and X-Ray Photoelectron Spectroscopy (Wiley, New York, 1983).
[8] Y.U. Idzerda, E.D. Williams, R.L. Park and J. Vähäkanas, Surface Sci. 177 (1986) L1028.
[9] A.E.T. Kuiper, G.C.J. van der Ligt, W.M. van de Wijgert, M.F.C. Willemsen and F.H.P.M. Habraken, J. Vacuum Sci. Technol. B 3 (1985) 830.
[10] C.D.Wagner, L.E. Davis, M.V. Zeller, J.A. Taylor, R.H. Raymond and L.H.Gale, Surface Interface Anal. 3 (1981) 211.
[11] M.P. Seah, Surface Interface Anal. 2 (1980) 222.
[12] D.A. Shirley, Phys. Rev. B 5 (1972) 4709.
[13] S. Tougaard, Surface Interface Anal. 11 (1988) 453.
[14] W.F. Egelhoff, Surface Sci. Rept. 6 (1987) 253.
[15] D.A. Shirley, Advan. Chem. Phys. 23 (1973) 85.
[16] M.P. Seah and W.A. Dench, Surface Interface Anal. 1 (1979) 2.
[17] C.J. Powell, Surface Sci. 44 (1974) 29.
[18] C.J. Powell, J. Vacuum Sci. Technol. A 3 (1985) 1338.
[19] C.J. Powell, Surface Interface Anal. 7 (1985) 263.
[20] W. Dolinski and H. Nowicki, Surface Interface Anal. 11 (1988) 229.
[21] C.W. Wagner, L.E. Davis and W.M. Riggs, Surface Interface Anal. 2 (1980) 53.
[22] F.J. Grunthaner and P.J. Grunthaner, Mater. Sci. Rept. 1 (1986) 69.
[23] F. Rochet, S. Rigo, M. Froment, C. D'Anterroches, C. Maillot, H. Roulet and G. Dufour, Advan. Phys. 35 (1986) 237.
[24] M.E. Levin, M. Salmeron, A.T. Bell and G.A. Somorjai, Surface Sci. 195 (1988) 429.
[25] C. Ocal and S. Ferrer, Surface Sci. 191 (1987) 147.

[26] K. Tamura, U. Bardi and Y. Nhei, Surface Sci. 197 (1988) L281.
[27] D.J. Dwyer, S.D. Cameron and J. Gland, Surface Sci. 159 (1985) 430.
[28] V.I. Nefedov and V.G. Yarzhemsky, J. Electron Spectrosc. Related Phenomena 11 (1977) 1.
[29] J.M. Scofield, J. Electron Spectrosc. Related Phenomena 8 (1976) 129.
[30] L.C. Feldman, J.W. Mayer and S.T. Picraux, Material Analysis by Ion Channeling (Academic Press, New York, 1982).
[31] L.R. Doolittle, Nucl. Instr. Methods Phys. Res. B 9 (1985) 344.
[32] L.E. Davis, N.C. MacDonald, P.W. Palmberg, G.E. Riach and R.E. Weber, Handbook of Auger Electron Spectroscopy (Perkin-Elmer, Eden Prairie, MN, 1978).